Comparison of soil excitation methods for surface wave speed measurements

M. Iodice[1], E. Rustighi[1], and J.M. Muggleton[1]
[1] University of Southampton, Institute of Sound and Vibration Research
Highfield Campus, SO17 1BJ, Southampton, United Kingdom
e-mail: **er@isvr.soton.ac.uk**

Abstract

Rayleigh waves are surface seismic waves, which can be produced by a disturbance applied to the surface of a half-space. The dispersive behaviour of Rayleigh waves in real multi-layered media is widely utilized for near-surface acoustic characterization, e.g. in Spectral Analysis of Surface Waves (SASW), and more recently, in Multi-channel Analysis of Surface Waves (MASW). These methods, along with the associated field testing, result in the construction of a dispersion curve. However, it is often difficult to measure the speed of Rayleigh waves in a consistent manner. Other interference, such as direct, reflected and refracted body waves, backscatter from nearby objects, are unwanted and could contaminate the dispersion curve (i.e. the phase velocity) in a significant way. Thus, shear or compression wave energy is undesirable. Furthermore, additional surface waves coming from other sources and background noise can compound the problems.

A wide range of different active sources have been utilized for decades in surface wave-based methods, but the reliability and the differences among these have not been properly assessed. The main focus of this paper is to compare different types of soil excitation, in order to identify and quantify seismic waves generated by each different type and to find a feasible Rayleigh wave source for the survey of shallow depths. This will be in terms of type of energy generated, range of frequencies excited, and amount of Rayleigh wave energy with respect to the total. Particularly, in this paper, the excitations caused by inertial shakers, oscillating in both the horizontal and vertical direction, and by transient sources like sledgehammers and mallets, are examined. For each different type of excitation, two key aspects are varied: the magnitude of the impact and the coupling of the source to the soil. The transmission of the energy from the source to the soil will be investigated using rigid platforms of different size, shape and material. This paper investigates the limitations of each type of active source to be utilized. These goals are pursued with experimental tests, digital processing of data, and by comparison with analytical and numerical models.

1 Introduction

Among all the methods utilised for the in-situ assessment of the bearing capacity (i.e. stiffness modulus) of soils and unbound layered material, and for the determination of the thickness of different layers and of geotechnical properties (e.g. shear modulus), non-destructive methods are universally accepted as reliable and advisable methods. Particularly, non-destructive in-situ seismic techniques such as Spectral Analysis of Surface Waves (SASW) and Multichannel Analysis of Surface Waves (MASW) seem to be very promising. Surface methods replaced the early seismic methods such as Cross-Hole, Down-Hole and Refraction/Reflection, because they are faster, less time-consuming and do not require boreholes to be dug [1] [2]. The principal aim of the surface methods is to evaluate the Rayleigh wave velocity, which depends on the shear wave velocity and the Poisson's ratio [3].

When a harmonic normal load is applied to the surface of a semi-infinite medium, more than two third of the total energy is transferred into Rayleigh wave-type [4] [5], thus this is the main component of the waves at the surface.

At a depth equal to approximately one wavelength, the amplitude of the Rayleigh wave is negligible, hence the displacements are small. It can be assumed that a wave with frequency f propagates within the material up to a depth of about one wavelength $\lambda_R = V_R / f$, where V_R is the Rayleigh wave velocity, and the final measurement is an average measure of the properties within a depth of one wavelength.

Spectral Analysis of Surface Waves (SASW) consists of a pair of receivers, typically geophones or accelerometers, spaced a distance D apart, and one source. Multichannel Analysis of Surface Waves (MASW) uses multiple receivers, but operates on the same principle. These methods consist of monitoring the propagation of Rayleigh waves over a wide range in wavelengths, at specified distances from the source. The vertical motion induced by the passage of the Rayleigh wave is recorded by means of transducers and a signal analyser at different distances from the source, and each time history is then transformed in the frequency domain via a Fourier Transform.

The requirement of a source is to excite a range of frequencies, dependent on the depth of the survey, the resolution required and the stiffness of the material being tested. Adequate amplitude has to be employed, so that waves can be detected also by furthest receivers. Seismic sources should be repeatable, in the terms that the amount and the time duration of the energy transmitted to the ground should not change at each test.

The source can be passive or active [6] [7]: passive sources do not generate energy artificially, but record the ground motion induced by background noise and micro-tremors, so they are not adjustable to fit case by case. They also usually do not provide high-frequency energy, hence they are utilised for deep depth investigations.

Active sources are typically classified as transient or continuous. Transient sources are excitations that last for a short finite period of time and they usually are impulsive, such as sledgehammers, mallets and falling masses, or even explosives [8] [9]. Continuous source are hydraulic or pneumatic vibrators and electro-mechanical shakers. The signal could either be a swept or a random signal [7] [10].

Sledgehammers used as impulsive sources are the most commonly utilized, allowing excitation of frequencies in a range dependent on the mass, but generally between about 15 and 200 Hz. In most of the cases the use of sledgehammers does not ensure that all the frequencies in the range are excited with proper amplitudes, i.e. some frequencies are missing, and the procedure is not precisely repeatable. In addition, the manual control of the amplitude of the force transmitted to the ground through a sledgehammer is extremely difficult [8].

To overcome these shortcomings, the use of continuous sources is preferable, because their energy emission spectrum is adjustable and so the frequency range is well-defined. They also have high repeatability.

One of the most critical characteristics of a source is its coupling to the soil [11]. Transient sources like falling masses which have large flat masses in contact with the ground are considered to be more desirable as Rayleigh wave sources than hammers on soil.

Despite their undoubted advantages, seismic techniques as MASW still have a few drawbacks and weaknesses [7] [6]: inclusion of noise, such as background noise, direct, reflected and refracted body waves; backscatter from nearby objects; other unwanted sources; and difficulties in performing real-time quality check of experimental data [6] [12] [13]. During the data acquisition process, the reliability of surface-wave methods lies in their capability to minimize noise inclusion [12].

However, it is difficult to generate only Rayleigh-type waves, but a variety of seismic waves are produced by ground excitation. Body waves could be refracted and reflected from boundaries due to a change in the material impedance, or could directly travel from the source to the receiver, in both cases contaminating the signal recorded. In addition, backscattered surface waves could exist, especially in the presence of buried discontinuities, such as building foundations or pipes.

Moreover, there is lack of standardisation, in terms of type of source to be used, coupling between source and the ground, experimental set-up to be adopted, and the receiver spacing.

The aim of this work is to compare different types of excitation and coupling, in order to define a feasible Rayleigh source for seismic wave methods, and understand their weaknesses and strengths. This goal is pursued through the collection of experimental data and the construction of a finite/infinite two dimensional element model of the ground which simulates the reality. The advantage of having a finite element model is that all the geometric and mechanical properties of the material are fixed and known, and there is absence of noise.

Furthermore, the source-receiver and receiver-receiver distances will be reviewed, as a validation and/or a breakdown of common rules of thumb.

2 Signal Processing for SASW/MASW and rules of thumb

Data processing in most of the seismic methods is made in the frequency domain, for its many advantages [9] [11].

The linear spectrum is a way of representing a periodic signal in terms of its frequency components, and it is used to identify the predominant frequencies and their absolute amplitudes and phases.

Signals from two records, $x(t)$ and $y(t)$, can be compared in terms of cross-power spectrum, which measures the inter-relationship between two signals in the frequency domain and it is defined as the average of the product of the spectrum of $x(t)$ and the complex conjugate spectrum of $y(t)$.

$$S_{xy}(f) = \lim_{T\to\infty} \frac{1}{T} E\left[S_x(f) \cdot S_y(f)^*\right] \tag{1}$$

Where $x(t)$ and $y(t)$ are the time histories of the signals, $S_x(f)$, $S_y(f)$ are the spectrums of the signals and (…)* denotes the complex conjugation operation.

The cross power spectrum carries the information of the relative phase between the two signals at each frequency within the bandwidth.

The auto-spectrum $S_{xx}(f)$ is the cross spectrum between the same signal $x(t)$ and is defined as the average of the raw spectrum:

$$S_{xx}(f) = \lim_{T\to\infty} \frac{1}{T} E\left[S_x(f) \cdot S_x(f)^*\right] \tag{2}$$

It describes how a random signal's power is decomposed as a function of frequency, e.g. it can be used to determine which band of frequencies makes the largest contribution to a signal.

The time delay between two receivers for each frequency component is then simply computed through the following expression, for each frequency:

$$t(f) = \frac{\arg(S_{xy}(f))}{2\pi \cdot f} \tag{3}$$

To reduce the background noise that obscure a signal coming from in-situ testing, averaging is a common and reliable practice. Averaging is possible as long as the system input is repeatable and the system is or can be considered linear. This is generally the case in the ground for small level of strains (typically less than $100\mu\varepsilon$) [14] [11].

It has been noticed that, in general, the arithmetic average of at least five signal records gathered under constant conditions is required [2].

The coherence function is defined as:

$$\gamma_{xy}^2 = \frac{|S_{xy}(f)|^2}{S_{xx}(f) \cdot S_{yy}(f)} \tag{4}$$

The coherence function is an absolute measure of how well the two signals $x(t)$ and $y(t)$ are linearly related. A coherence value close to unity at a certain frequency corresponds to a perfect correlation between the two signals, while a coherence value close to zero means that the two signals are totally unrelated. Coherence is the most common method to perform real time quality checks, i.e. to see the level of noise contamination [15].

Surface waves travel horizontally only after a certain distance, called near-offset, when surface-type waves are influenced by body waves and do not have planar propagation [6]. An empirical rule of thumb to avoid this unwanted effect, is widely proven to be:

$$x_1 \geq 0.5 \cdot \lambda_{\max} \tag{5}$$

Where:

x_1 is the offset between source and the first receiver

$\lambda_{\max}$ is the maximum desired wavelength

Spacing between receivers depends on the desired wavelength to be measured and on the elastic properties of the soil to be tested. In terms of spatial distribution of receivers, the most accepted empirical rule of thumb is the following [11] [15]:

$$\frac{\lambda}{3} \leq D \leq 2\lambda \tag{6}$$

The lower bound is a due to the precision of the instrumentation which creates a physical limitation that governs the spacing between geophones. The upper bound is an empirical criterion tailored to avoid the far-offset effect, which is the attenuation of the Rayleigh wave high-frequency energy, and the consequent contamination by body waves high-frequency components [6]. Far-offset effects limit the highest frequency at which the phase angle can be still measured without incurring in any errors, so the upper bound of receiver spacing should be tailored to insure that the Rayleigh-wave energy does not decay excessively.

The receiver spacing is also governed by the equivalent in the space domain of the Nyquist sampling criterion, in order to avoid spatial aliasing:

$$D \leq \frac{\lambda}{2} \tag{7}$$

Therefore, many authors proposed different empirical criteria, and there is not a standard about the experimental set-up for MASW technique [16]. The debate over the optimum configuration contributes to the lack of standardization of surface-wave methods, slowing down their use.

3 Experimental Investigation

In order to collect enough reliable data and to better understand the differences among different types of excitation, a series of experiments have been carried out to determine the variability of the wave speed over a small volume of ground. For this purpose a private test site which belongs to the University of Southampton, based on the northern side of the town, has been exploited. The test site soil is mainly composed of a soft 20 cm upper layer and a stiffer clayey layer.

3.1 Experimental procedure

The experimental set-up consisted of a source and an array of 8 triaxial geophones. The data was acquired using a ProSig P8020 data acquisition unit and a laptop. In the following experimental investigation all the results are recorded 5 times with a sample frequency of $8KHz$ and duration of $2\sec$, under the same input conditions, and then averaged in the frequency domain.

The spacing is shown in the Figure 1, where G refers to geophone and the number identifies the position. Distances are shown in meters.

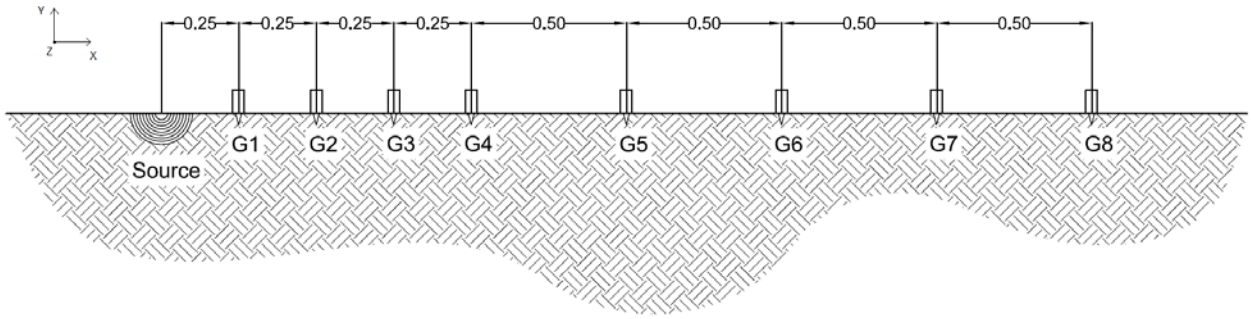

Figure 1: Experimental set-up (distances are in metres)

Different types of sources have been evaluated, both transient and continuous, with different source-to-ground coupling and different directions of excitation. For the impulsive excitations, the ground has been directly struck by means of a metallic mallet, while for the transient excitations an IV40 Data Physics inertial shaker has been used. Different steel platforms have been used in order to assess different couplings:

- One rectangular L-shaped aluminium platform, with horizontal plate 16.0x16.0x1.5 cm and vertical plate 10.0x16.0x1.5 cm. To ensure a good source-to-ground coupling, this platform has 2 mounts attached, 7.5 cm each long, which penetrate into the ground and could be alternatively oriented parallel or normally to the array of the survey, or completely removed.
- One aluminium circular plate with $\varnothing = 15cm$ and thickness equal to $1.5cm$, laid down the ground.
- One aluminium circular plate with $\varnothing = 30cm$ and thickness equal to $1.5cm$, laid down the ground.

The shaker could be bolted to the rectangular platform in two different ways, in the horizontal and in the vertical direction with respect to the ground surface, while could be only attached vertically to the circular plates.

Figure 2 shows the L-shaped platform, in its orthogonal configuration, with the shaker bolted horizontally and vertically.

The differences in the coupling between source and ground have been evaluated also fusing a layer of mono-granular sand prepared between the platform and the ground. All the different excitation methods which have been experimentally and/or numerically investigated in this paper are depicted in Figure 3.

For the continuous sources, the magnitude of the load is measured through a force gage mounted between the platform and the shaker, and by means of an accelerometer directly mounted on the bottom of the shaker chassis. The nominal moving mass of the IV40 body is 1.21kg, so the force could be easily computed as the product of the moving mass times the acceleration.

The time extended signal is white noise, with a unit variance and low pass filtered at $4KHz$, so to avoid aliasing. The peak force value is about $0.015N$. Seismic methods use linear elastic theories to associate

measurements with mechanical properties of the material being tested, and this is true only for low level of strain (less than $100\mu\varepsilon$) [14].

In the experimental investigation all the excitations showed in Figure 3 have been tested, with the exception of the number 12.

Figure 2: rectangular platform with shaker attached horizontally (a) and vertically (b)

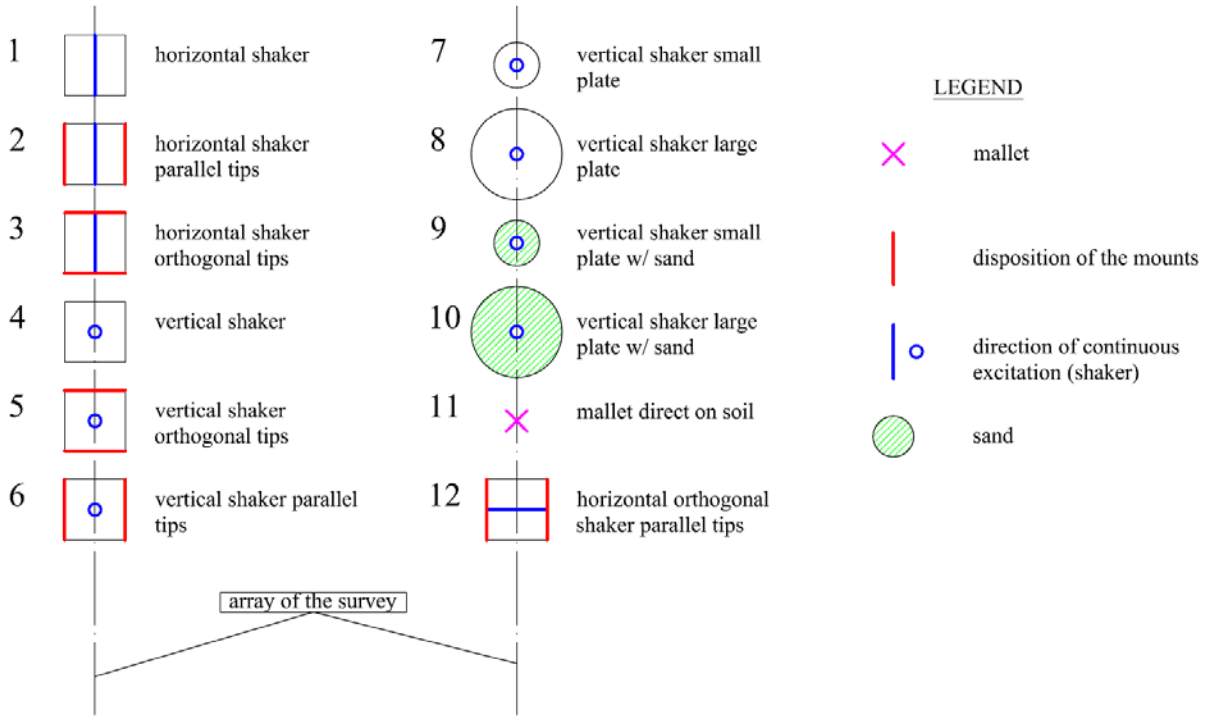

Figure 3: The 12 different types of excitation (top view)

3.2 Experimental results

Considering the phase difference $\phi(f)$ between the vertical displacements signals recorded at two different positions, the travel time is computed through (3).

The phase velocity is obtained using the following expression:

$$V_{ph} = \frac{D \cdot 2\pi \cdot f}{\phi(f)} \tag{8}$$

This leads to the construction of a dispersion curve for the material tested, if the same procedure is repeated for each applied frequency in the acceptable range, and for each possible receiver spacing.

It can be observed that the Rayleigh phase velocity computed by (8) is an averaged value of the entire volume of material investigated between two receivers [14].

Figures 4 depicts the phase angle values obtained with all the different types of excitation mentioned in section 3.1, between geophone 1 and geophone 5. Figure 5 depicts the phase angle values obtained between geophone 3 and geophone 5. The spacing have been chosen as example illustrations only.

While the phase angle for the vertical excitation methods seems to manifest the same slope with frequency, the phase angle computed through horizontal methods shows a significant change in slope, from about 100Hz (shown by the vertical line).

Possibly, horizontal methods produce also body wave energy, which results in a change in the slope for higher frequencies, due to the far-field effect, when the high frequency Rayleigh-type energy is dissipated and is therefore dominated by body wave energy. Vertical excitation methods (number 4, 5, 7, 8, 9, 10) seem to suffer less from that phenomenon.

Comparing the two figures it can be noticed that, further away from the source, the threshold differs: around 100 Hz for the phase between geophone 1 and 5 (Figure 4) and around 65 Hz for the phase between geophone 3 and 5 (Figure 5), i.e. higher Rayleigh wave frequencies have a faster geometrical damping.

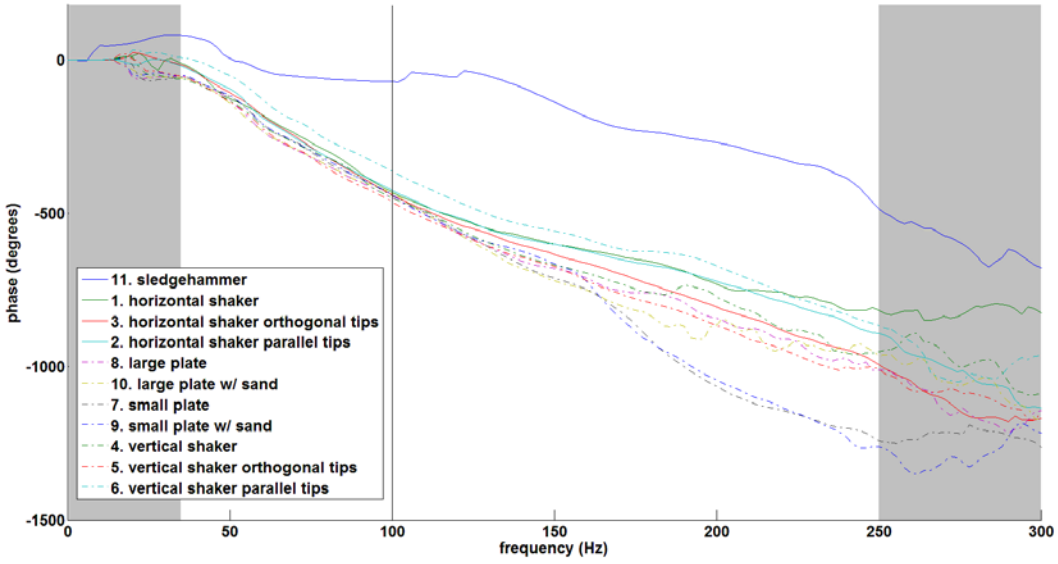

Figure 4: Unwrapped phase vertical component between geophone 1 and geophone 5

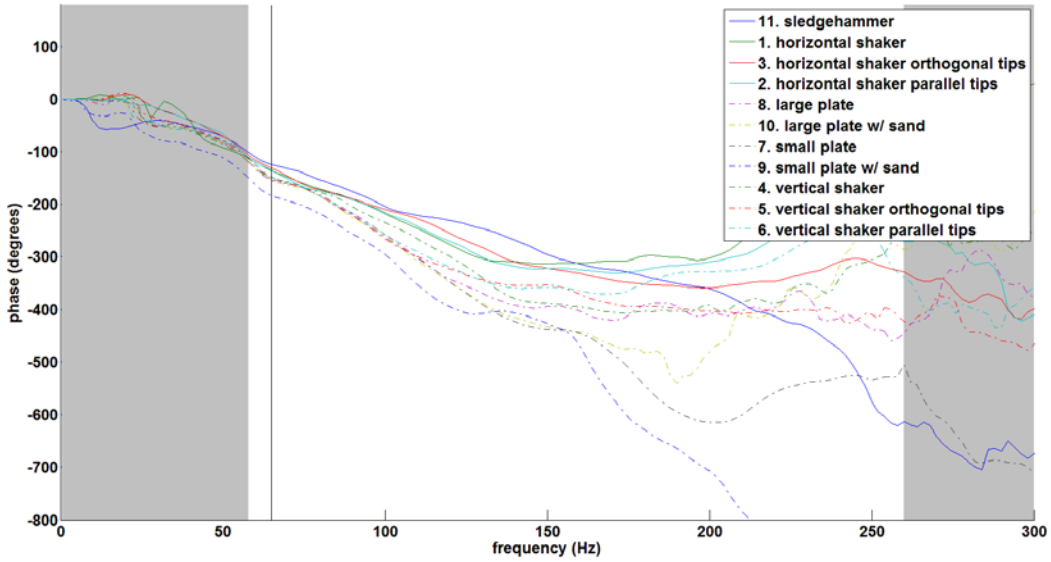

Figure 5: Unwrapped phase vertical component between geophone 3 and geophone 5

The shaded area displays the lower bound for the reliable frequency range, according to (6), and the upper bound, for the frequencies associated with poor coherence values (less than 0.2). The lower bound seems to fit for the first receiver spacing, while it seems to be too restrictive for smaller receiver spacings.

There are no big differences among couplings, but mounts disposed orthogonally to the array of the survey (excitation number 3) seem to have an intermediate behaviour, so a higher level of surface-wave energy and less attenuation manifest. No clear differences are noticeable between circular or rectangular shaped platform, but large circular plate is more advisable than small circular plate as a source to ground coupling, since the linear trend of the phase in case of small plate away for lower frequencies (Figure 4). A layer of sand dampens the system, so the upper bound of reliable frequency slightly diminishes: it can be noticed in both figures, since the linear trend of the phase in case of sand fades away for lower frequencies.

The impulsive method (number 11) has low repeatability and its reliability depends on the similarity, in terms of amplitude, between different strokes: the poor reliability manifests in a non-linear trend of the phase angle, at least for the spacing between geophone 1 and geophone 5 (Figure 4).

4 Numerical Validation

Alongside the experimental investigation, and as a validation of it, a two-dimensional finite/infinite element model of the ground has been assembled through the Abaqus/CAE software, in the X-Y plane, for modelling the seismic waves in a semi-infinite half space. This model is subject to a number of assumptions. The medium is considered to be elastic, isotropic and homogeneous. The biggest issue with numerical simulation of the dynamic response of an infinite ground is to avoid, or at least minimize, the effects of reflection of the wave fronts from the boundaries, and hence to properly model P-wave, S-wave and Rayleigh surface waves [17]. In this research, both finite and infinite elements are used in the simulations: infinite elements are often used in combination with finite elements to model an unbound problem without reflections from the domain boundaries. Infinite elements behave as many infinitesimal dashpots which are oriented normally and tangentially with respect to the boundary, so that stress is proportional and in phase with the rate of strain.

Plain-strain finite elements have been used for the ground simulation: it means that the strain normal to the X-Y plane, ε_z, and the shear strain γ_{xz} and γ_{yz}, are assumed to be very small.

With finite elements methods, two discretization constraints should be adopted in order to achieve appropriate spatial and temporal resolution. The spatial condition assures that a sufficient number of points in space are sampled in order to recreate the wave, or in other word that the element size $l_{\max}$ is small enough (it is the analogue of the Nyquist's criterion in the time domain) [18].

$$l_{\max} \leq \left(\frac{1}{8} \div \frac{1}{5}\right)\lambda_s \tag{9}$$

Where $\lambda_s = \frac{c_s}{f_{\max}}$ is the minimum wavelength and c_s is the S-wave speed. Rearranging (9) we obtain a relationship between the element size and the upper limit of the frequency range:

$$f_{\max} \leq \left(\frac{1}{8} \div \frac{1}{5}\right)\frac{c_s}{l_{\max}} \tag{10}$$

The temporal constraint must be set after the spatial, to ensure that the wave front does not travel faster than the time step Δt. This is achieved using the Curant condition [19] [20], here rearranged for two-dimensional problems (c_p is the P-wave speed):

$$\Delta t_{\max} \leq \frac{1}{c_p\sqrt{\frac{1}{l_{\max}{}^2}}} \tag{11}$$

Acoustic elements have also been used in order to simulate the excitation method normal to the array of the survey (n.12): they have one active degree of freedom, which is the acoustic pressure at each single node. An acoustic analogy has been exploited to extract the displacements in the Z direction from the two-dimensional model: in fact the fundamental equation of motion for an elastic half space excited by a line source of infinite length vibrating on a free surface, with the direction of vibration parallel to the length of the source, is expressed by a wave equation [5].

Table 1 depicts the features of the elements used in the model.

TYPE	NAME	DESCRIPTION	DOF
Finite	CPE3	3-node linear plane-strain triangle	Translation in direction x,y
Infinite	CINPE5	5-node bilinear plane-strain quadrilater	Translation in direction x,y
Acoustic	AC2D3	3-node linear 2D acoustic triangle	Acoustic pressure

Table 1: Features of the elements used in the model

4.1 Features of the 2D model

The model consists of a two-dimensional semicircular 50 meters radius half-space, with infinite elements applied on the circular boundary. The shape has been chosen due to the importance of the position of the nodes in the infinite direction with respect to the origin. In fact infinite elements only give perfect absorption for perpendicularly impinging waves, so a circular shape ensures that that the vectors of the circular wave-front propagating wave are almost normal to the boundary. Simulations have been run with the parameters of Table 2. The mechanical parameters have been chosen to be close enough to typical values for the ground, and are not so different from that used in [17].

Young's Modulus, E	$100 \cdot 10^6 Pa$
Shear Modulus, G	$376 \cdot 10^5 Pa$
Poisson ratio, ν	0.33
Viscous damping, α	0
Rayleigh damping, β	$0.2/200 \cdot 2\pi$
Mass density, ρ	$2000 Kg \cdot m^{-3}$
Rigid body half-width, $a/2$	$0.05m$
Maximum element size on the surface, $l_{\max}$	$0.05m$
Finite model size, R	$50m$
Maximum time step, $\Delta t_{\max}$	$5 \cdot 10^{-5}$ sec
Duration of the simulation T	0.25sec

Table 2: Model parameters

The values for the seismic wave speeds are (c_r is the speed of the Rayleigh wave):

$$c_p \approx 272 \frac{m}{s} \; c_s \approx 137 \frac{m}{s} \; c_r \approx 128 \frac{m}{s} \tag{12}$$

Since we are only interested in surface wave measurements, the size of the finite elements is maintained constant and equal for the first 5 meters of the radius on the surface, increasing then with depth and with distance. The duration of the simulation ($T = 0.25\text{sec}$) ensures the absence of reflected waves for a semi-circular region of 30 meters of radius, in the case the contribution of the infinite element is not considered.

Classical Rayleigh damping uses a system damping matrix $\underline{C}$ proportional to the mass and stiffness matrices as follows [21]:

$$\underline{C} = \alpha \underline{M} + \beta \underline{K} \tag{13}$$

Where:

α is the mass-proportional damping coefficient

β is the stiffness-proportional damping coefficient

Relationships between the modal equations and orthogonality conditions allow this equation to be rewritten as:

$$\xi = \frac{1}{2\omega_n} \alpha + \frac{\omega_n}{2} \beta \tag{14}$$

Where:

ξ is the damping ratio

ω_n is the natural frequency

It can be noticed that the damping ratio varies with natural frequency. The values of α and β are usually selected, according to engineering estimations, such that the critical damping ratio is given at two known frequencies. In the following simulations the critical damping ratio has been chosen so to vary linearly from 0 at 0 Hz to 0.2 at 200 Hz, and the α coefficient was assumed to be zero.

When using acoustic elements, according to the acoustic analogy, the value of the bulk modulus becomes the value of the shear modulus.

Rigid bodies have been used in order to simulate the different types of platform and mounts used in the series of experiments. Rigid body nodes have been used to constrain the motion of selected points, so that their relative position from a reference point (RP) remains constant throughout the analysis, prohibiting deformation. Rigid bodies have a surface of width a.

4.2 Analytical validation of the 2D model

The results coming from the 2D model have been validated through the analytical results proposed by Miller and Pursey [22] and Graff [5]. The types of source considered for the numerical validation of the model are:

a) "an infinitely long strip of fine width vibrating in a direction normal to the surface of the medium"
b) "an infinitely long strip of finite width vibrating tangentially to the surface of the medium and normally to the axis of the strip"

The boundary conditions fixed by the authors [22] to obtain the results are: a normal harmonic load with unit amplitude for case (a) and a shear harmonic load with unit amplitude for case (b). The results are, for case (a), with $\nu = 0.33$:

$$u_x(x,0) \approx 0.198 \cdot \frac{a}{\mu} \exp(-2.145ikx) \cdot \exp(-k\xi x) \tag{15}$$

$$u_y(x,0) \approx 0.311 \cdot \frac{ia}{\mu} \exp(-2.145ikx) \cdot \exp(-k\xi x). \tag{16}$$

Where:

u_x are the displacements in the horizontal direction

u_y are the displacements in the vertical direction

a is the width of the finite vibrating line

x is the desired position in the X-direction

$k = \frac{\omega}{c_p}$ is the wavenumber of the body wave

ξ is the damping ratio

And for (b), with $\nu = 0.33$:

$$u_R \approx \frac{a}{\mu} \exp\left(i\left(\frac{3\pi}{4} - kR\right)\right) \cdot \left(\frac{2}{\pi R}\right)^{\frac{1}{2}} \cdot \frac{\sin 2\theta (c^2 - \sin^2\theta)}{F_0(\sin\theta)} \cdot \exp(-k\xi x), \tag{17}$$

$$u_\theta \approx \frac{a}{\mu} \exp\left(i\left(\frac{3\pi}{4} - ckR\right)\right) \cdot \left(\frac{2c^7}{\pi R}\right) \cdot \frac{\cos\theta \cos 2\theta}{F_0(c\sin\theta)} \cdot \exp(-k\xi x) \tag{18}$$

Where:

$u_R \approx u_y \cos\theta + u_x \sin\theta,$

$u_\theta \approx u_x \cos\theta - u_y \sin\theta$

R is the radial distance from the source

θ is the angle from the vertical axis

$$c^2 = \frac{(\lambda + 2\mu)}{\mu}$$

μ, λ are the Lame constants

k is the wavenumber of the body wave

ξ is the damping ratio

$$F_0 = (2k^2 - c^2)^2 - 4k^2(k^2 - 1)^{\frac{1}{2}}(k^2 - c^2)^{\frac{1}{2}}$$

And, for the surface waves solution, $\theta = \frac{\pi}{2}$.

Two different simulations have been carried out with the model, with a uniform-distributed sinusoidal windowed burst load, $f(t)$, acting normally to the surface (case a) and tangentially (case b), uniformly distributed on a surface of finite width a.

The load has been multiplied by a windowing function (Hann window in this case) in order to minimize the effects in terms of displacements of an instantaneous growth of the load.

In Figure 6 one can notice the comparison between the analytical solution and the numerical model in terms of phase angle between the source load and the signal at different position away from the source. The phase angle has been computed taking into account vertical/horizontal displacements obtained for case (a). It can be noticed that the normal load on an infinite line of finite width gives a good estimation of the Rayleigh wave velocity c_r, for both vertical and horizontal displacements. The model seems to work with good agreement with the analytical results.

In Figure 7 one can notice the comparison between the analytical solution and the numerical model in terms of phase angle between the source load and the signal at different position away from the source. The phase angle has been computed taking into account vertical/horizontal displacements obtained for case (b). It can be noticed that the long strip vibrating tangentially on an infinite line of finite width gives a good estimation of the shear wave velocity c_s concerning vertical displacements, while gives an overestimation of c_s, or a underestimation of c_p if the horizontal displacements are considered for the computation of the phase angle. One can notice, again, that the results coming from the model match fairly well the analytical results, thus the two-dimensional model can be considered a reliable tool to simulate different types of excitation.

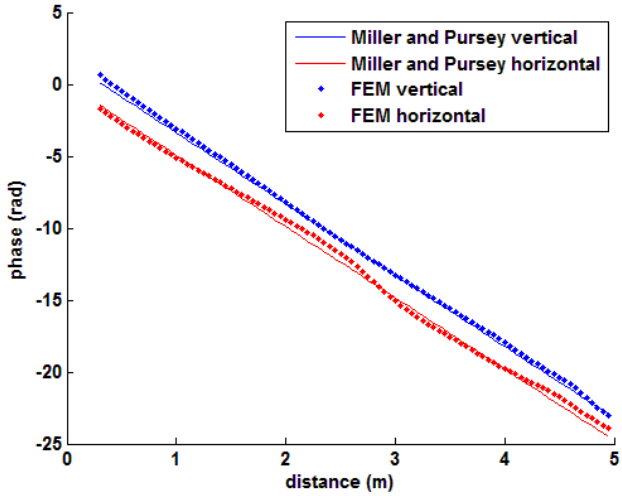

Figure 6: Comparison between phase angle from analytical solution and from FEM, case (a) of normal load

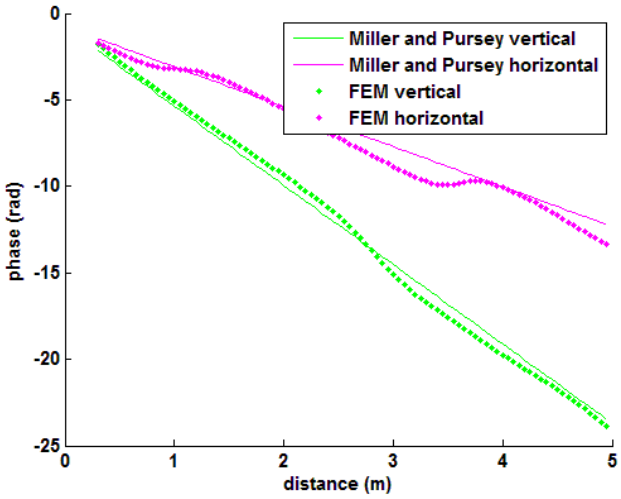

Figure 7: Comparison between phase angle from analytical solution and from FEM, case (b) of tangential load

4.3 Numerical investigation of sources for MASW

An impulse force $f(t)$ has been used in the simulation, evenly distributed along the surface of the rigid body. When simulating the vertical load, the $f(t)$ is applied normally to the surface. When simulating the horizontal load, the $f(t)$ is applied tangentially to the surface and a moment $m(t) = a \cdot f(t)$, acting normally to the Z-direction, is also applied at the reference point (RP), i.e. at the centre of the surface, where the $a = 0.05$ is the arm of the moment. Figure 9 shows the load $f(t)$.

For the excitation method normal to the array of the survey (n.12), a pressure uniformly distributed to the finite width line has been used: the time history is also shown in Figure 9. Remembering the acoustic analogy, it corresponds to infer a displacement in the Z-direction.

In the numerical simulation, the excitation methods that have been tested, according to Figure 3, are the number 1, 2, 3, 4, 5, 6, 11, 12. Figure 9 shows the phase difference between the time histories of vertical displacements (Y-direction) recorded at two nodes on the surface of the model, respectively 0.50 m and 2.00 m far from the source. One can notice that there is a difference in slope between the horizontal-based and the vertical-based methods: the vertical methods lead to the biggest absolute values for the phase angle difference, while horizontal based methods lead to smaller values of the phase angle. An intermediate behaviour can be noticed for the excitation method normal to the array of the survey (n.12), where the phase angle is computed considering the displacements in the Z-direction.

The differences between different couplings are minimal, as each excitation method almost overlaps all the methods belonging to same direction of excitation.

Figure 10 shows the difference in terms of phase velocity between the same two points, as computed from (4). The dashed horizontal lines refer to the velocity of P-wave, S-wave and R-wave (12). It can be noticed that vertical methods lead to the assessment of the R-wave speed with good accuracy, while the horizontal methods overestimate the R-wave phase velocity, probably due to their amount of body wave energy. The excitation method normal to the array of the survey (n.12) shows an intermediate behavior and leads to the assessment of the S-wave speed. The estimation of R-wave velocity for the vertical-based excitation has a good accuracy, with a percent of error under 8% in the frequency range between 100 Hz and 350 Hz, The excitation method n.12 estimates the S-wave speed with good accuracy: the percent of error in the frequency range between 100 Hz and 350 Hz is under 4%.

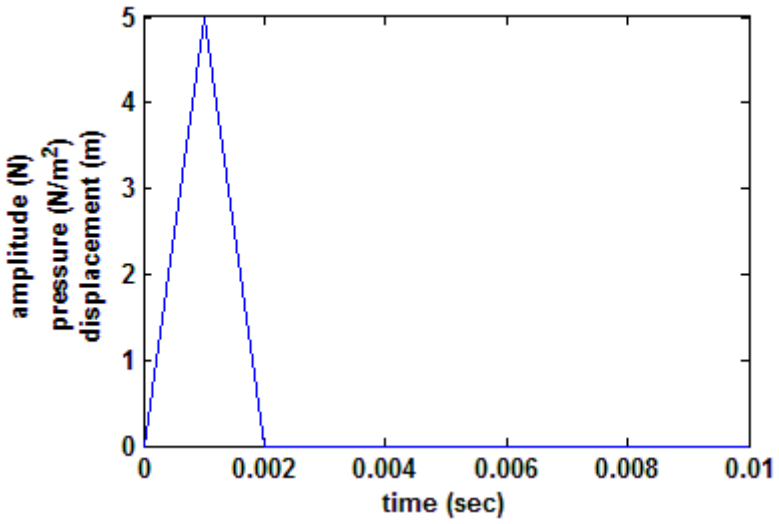

Figure 8: Time history of force/pressure for the impulsive load used in the simulations

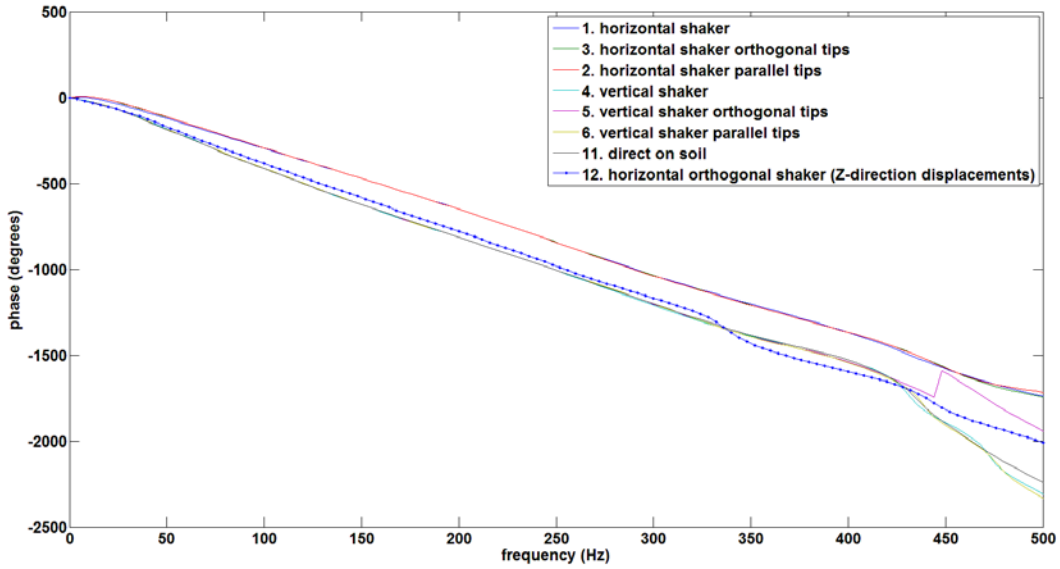

Figure 9: Comparison phase angle difference between vertical and horizontal excitations in the FEM (node 427-node 397)

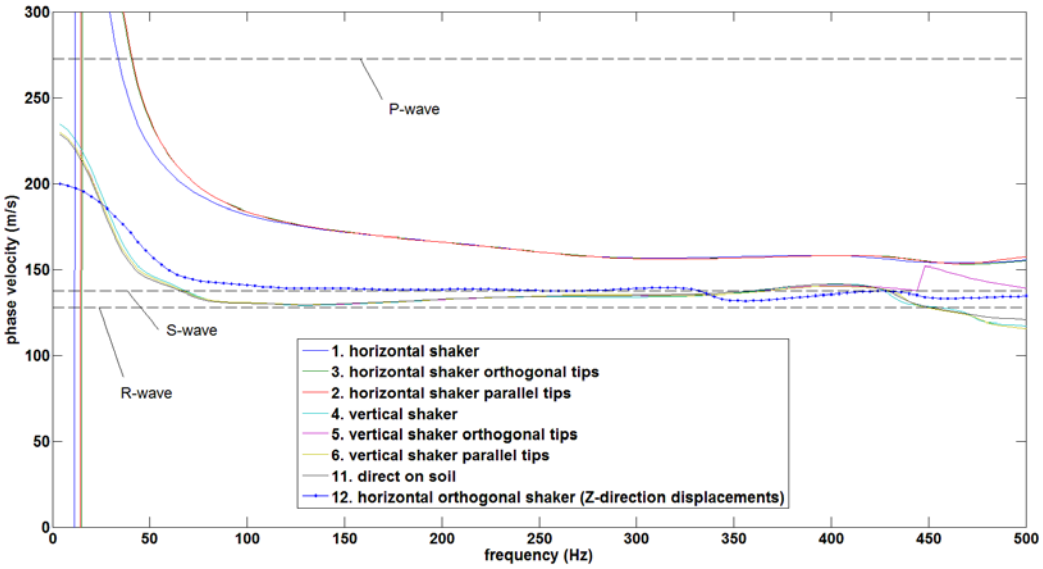

Figure 10: Comparison phase velocity between vertical and horizontal excitations in the FEM (node 427-node 397)

5 Conclusions

Different testing methods for seismic surveys have their qualities and limitations. Vertical excitation methods seem to have high reliability to estimate the Rayleigh wave velocity in soils. Horizontal excitations produce also a significant amount of compressional wave energy causing a wrong estimation of the Rayleigh wave phase velocity, from a frequency threshold which becomes lower going away from the source. A horizontal source which could transmit a shear force to the ground, minimizing the transmission of any moment, could be an objective for future works and could allow measuring the shear wave velocity in a direct way. A direct comparison between the behaviour of soil and the data coming from the model is the following step to pursue.

Acknowledgments

The authors gratefully acknowledge the financial support of the UK Engineering and Physical Sciences Research Council under grant EP/K021699 “Assessing the Underworld – an integrated performance model of city infrastructures”.

References

[1] G.C. Lai, *Spectral Analysis of Surface Waves Active Methods Technical Recommendations*, Rivista Italiana di Geotecnica, 4/2000.

[2] S. Nazarian and K. Stokoe, *Evaluation of moduli and thicknesses of Pavement System by Spectral-Analysis-of-Surface-Waves Methods*, No. FHWA-TX-83-26+ 256-4 Intrm Rpt., The Center, 1983.

[3] J. Houbrechts, M. Schevenels, G. Lombaert, G. Degrande, W. Rücker, V. Cuellar, A. Smekal, *Test Procedures for the Determination of the Dynamic Soil Characteristics*, 2011.

[4] R.D. Woods, *Screening of Surface Waves in Soils*, Woods, Am Soc Civil Engr J Soil Mech (1968).

[5] K.F. Graff, *Wave Motion in Elastic Solids*, Courier Dover Publications, 1975, pp 344-356.

[6] C.B. Park, R.D. Miller, J. Xia, *Multichannel Analysis of Surface Waves*, Geophysics 64.3 (1999): 800-808.

[7] S. Nazarian, *Shear Wave Velocity Profiling with Surface Waves Methods*, *Geotechnical Engineering State of Art and Practice: Keynote Lectures from GeoCongress 2012*, pp.221-240.

[8] J. Kumar and P.G. Rakaraddi, *SASW evaluation of asphaltic and cement concrete pavement using different heights of fall for a spherical mass*, International Journal of Pavement Engineering 14.4 (2013): 354-363.

[9] K. Stokoe and S. Nazarian, *Use of Rayleigh waves in liquefaction studies*, Measurement and use of shear wave velocity for evaluating dynamic soil properties, ASCE, 1985.

[10] B. Menzies, *Near-surface characterisation by ground stiffness profiling using surface waves geophysics*, Instrumentation in Geotechnical Engineering, HC Verma Commemorative Volume (2001): 43-71.

[11] J.S. Heisey, K.H. Stokoe, W.R. Hudson, A.H. Meyer, *Determination of in Situ Shear Wave Velocities from Spectral Analysis of Surface Waves*, No. FHWA/TX-82/34+ 256-2 Intrm Rpt., 1982.

[12] C.B. Park, R.D. Miller, J. Xia and J. Ivanov, *Seismic Characterization of Geotechnical Sites By Multichannel Analysis of Surface Waves (MASW) Method, Tenth International Conference on Soil Dynamics and Earthquake Engineering (SDEE), Philadelphia*, 2001.

[13] C.B. Park, R.D. Miller, J. Xia and J. Ivanov, *Multichannel Seismic Surface-Wave Methods for Geotechnical Applications*, *Proceedings of the First International conference on the application of geophysical methodologies to transportation facilities and infrastructure,* St. Louis, 2000.

[14] R. Luna, H. Jadi, *Determination of Dynamic Soil Properties Using Geophysical Methods, Proceedings of the First International Conference on the Application of Geophysical and NDT Methodologies to Transportation Facilities and Infrastructure—Geophysics*, Vol. 2000, 2000.

[15] S. Foti, S. Parolai, D. Albarello, M. Picozzi, *Application of Surface-wave methods for seismic site characterization*, Surveys in geophysics, 32.6 (2011): 777-825.

[16] A. Goel and A. Das, *A Brief Review on Different Surface Wave Methods and Their Applicability for Non-Destructive Evaluation of Pavements.*

[17] K. Edip, M.Garevski, V. Sesov, C. Butenweg, *Numerical simulation of wave propagation in soil media, 21st European Young Geotechnical Engineers Conference*, 2011.

[18] R.L. Kuhlemeyer, and J. Lysmer, *Finite element method accuracy for wave propagation problems,* Journal of Soil Mechanics & Foundations Div 99.Tech Rpt (1973).

[19] C.T. Schroeder, W.R. Scott, Jr., *A finite-difference model to study the elastic-wave interactions with buried land mines,* Geoscience and Remote Sensing, IEEE Transactions on 38.4 (2000): 1505-1512.

[20] C.T. Schoreder, *On the interaction of elastic waves with buried land mines: an investigation using the finite-difference time-domain method*, (2001).

[21] E.L. Wilson, *Static and Dynamic Analysis of Structures* (4th ed.). Berkeley, CA: Computers and Structures, Inc, 2004.

[22] G.F. Miller and H. Pursey, *The field and radiation impedance of mechanical radiators on the free surface of a semi-infinite isotropic solid*, *Proceedings of the Royal Society of London. Series A. Mathematical and Physical Sciences* 223.1155 (1954): 521-541.